Nuclear Instruments and Methods in Physics Research A 340 (1994) 594–604
North-Holland

NUCLEAR INSTRUMENTS & METHODS IN PHYSICS RESEARCH
Section A

Generalization of the Zgoubi method for ray-tracing to include electric fields

F. Méot [1]

Groupe Théorie, Laboratoire National SATURNE, DSM-CEA & IN2P3-CNRS, CE Saclay, 91191 Gif-sur-Yvette Cedex, France

(Received 1 June 1993; revised form received 1 October 1993)

The ray-tracing and spin tracking code Zgoubi, originally dedicated to the numerical integration of Lorentz equation in magnetic fields, has been improved in order to allow ray-tracing in electric and electromagnetic fields. This report describes the method, and presents detailed examples of application, including the achromatic quadrupole.

1. Introduction

In its basic version, the ray-tracing code Zgoubi [1] calculates particle trajectories by numerical step by step integration of motion in magnetic fields, following the law

$$\mathrm{d}\boldsymbol{p}/\mathrm{d}t = q\boldsymbol{v}\times\boldsymbol{b}, \tag{1}$$

($\boldsymbol{p}$ = impulse, t = time, q = charge, $\boldsymbol{v}$ = velocity, $\boldsymbol{b}$ = magnetic field). In order to enable dealing with electrostatic lenses, or combined electromagnetic optical elements, the ingredients necessary for the treatment of the complete Lorentz equation

$$\mathrm{d}\boldsymbol{p}/\mathrm{d}t = q(\boldsymbol{e}+\boldsymbol{v}\times\boldsymbol{b}), \tag{2}$$

($\boldsymbol{e}$ = electric field) have been added to the existing code.

The code Zgoubi also provides spin-tracking [2], but considering the negligible effect of electric fields on the spin motion, the treatment of the Thomas–BMT equation has not been modified.

2. Principles of the method

The method of integration remains the same as in the basic version, namely it uses Taylor expansions in the vicinity of initial conditions, in the following way. The Eq. (2) above is normalized for easier handling, by taking $\boldsymbol{p} = qB\rho\boldsymbol{u}$, $B\rho$ = rigidity, $\boldsymbol{u} = \boldsymbol{v}/v$, $\mathrm{d}s = v\mathrm{d}t$, $\boldsymbol{u}' = \mathrm{d}\boldsymbol{u}/\mathrm{d}s$, which leads to

$$(B\rho)'\boldsymbol{u} + B\rho\boldsymbol{u}' = \frac{\boldsymbol{e}}{v} + \boldsymbol{u}\times\boldsymbol{b}. \tag{3}$$

From vector position $\boldsymbol{R}(M_0)$ and unit velocity $\boldsymbol{u}(M_0)$ at point M_0, the position $\boldsymbol{R}(M_1)$ and unit velocity $\boldsymbol{u}(M_1)$ at point M_1 following a displacement $\mathrm{d}s$ are obtained from Taylor expansions (Fig. 1)

$$\begin{aligned}\boldsymbol{R}(M_1) &= \boldsymbol{R}(M_0) + \boldsymbol{u}(M_0)\,\mathrm{d}s + \cdots + \boldsymbol{u}''''(M_0)\frac{\mathrm{d}s^6}{6!}\\ \boldsymbol{u}(M_1) &= \boldsymbol{u}(M_0) + \boldsymbol{u}(M_0)\,\mathrm{d}s + \cdots + \boldsymbol{u}''''(M_0)\frac{\mathrm{d}s^5}{5!}\end{aligned} \tag{4}$$

and the rigidity at M_1 is obtained in the same way from

$$B\rho(M_1) = B\rho(M_0) + (B\rho)'(M_0)\,\mathrm{d}s + \cdots + (B\rho)''''(M_0)\frac{\mathrm{d}s^4}{4!}. \tag{5}$$

The derivatives $\boldsymbol{u}^{(n)} = \mathrm{d}^n\boldsymbol{u}/\mathrm{d}s^n$ and $(B\rho)^{(n)} = \mathrm{d}^nB\rho/\mathrm{d}s^n$ are obtained in three different ways, depending on whether $\boldsymbol{e}$ or $\boldsymbol{b}$ is zero as described in the next three sections. The reason for this decoupling, when just the general case ($\boldsymbol{e}$ and $\boldsymbol{b}$ non-zero) could be considered, is the sake of computing speed.

2.1. Integration in magnetic fields

This section is a reminder of the basic content of the code, which has already been described in detail in other reports [2]. Considering that $\boldsymbol{e}\equiv 0$, the (normalized) Lorentz Eq. (3) reduces to

$$\boldsymbol{u}' = \boldsymbol{u}\times\boldsymbol{B}, \tag{6}$$

where $\boldsymbol{B} = \boldsymbol{b}/B\rho$. Successive differentiations lead to

$$\begin{aligned}\boldsymbol{u}'' &= \boldsymbol{u}'\times\boldsymbol{B} + \boldsymbol{u}\times\boldsymbol{B}',\\ \boldsymbol{u}''' &= \boldsymbol{u}''\times\boldsymbol{B} + 2\boldsymbol{u}'\times\boldsymbol{B}' + \boldsymbol{u}\times\boldsymbol{B}'',\end{aligned} \tag{7}$$

[1] Present address: CERN/SL/AP, F-01631 CERN Cedex.

SSDI 0168-9002(93)E1204-B

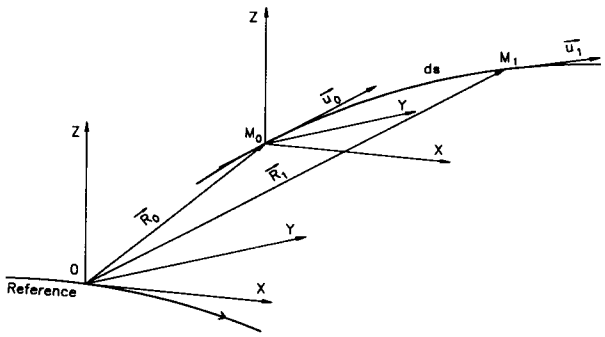

Fig. 1. Reference frame and coordinates used in Zgoubi.

and so on, up to the 5th order derivative $\boldsymbol{u}'''''$, where the derivatives $\boldsymbol{b}^{(n)} = \mathrm{d}^n\boldsymbol{b}/\mathrm{d}s^n$ of the magnetic field are calculated from the vector field $\boldsymbol{b}(x, y, z)$ and its derivatives $\partial^{i+j+k}\boldsymbol{b}(x, y, z)/\partial x^i\partial y^j\partial z^k$ up to the fourth order, provided explicitly by dedicated routines of the code (namely those routines that deal with field maps, or provide the analytical models of optical elements).

2.2. Integration in combined electric and magnetic fields

When both $\boldsymbol{e}$ and $\boldsymbol{b}$ are non-zero, the complete Eq. (3) must be considered. Successive differentiations give the following recursive relations

$$
\begin{aligned}
&(B\rho)'\boldsymbol{u} + B\rho\boldsymbol{u}' = \frac{\boldsymbol{e}}{v} + \boldsymbol{u}\times\boldsymbol{b},\\
&(B\rho)''\boldsymbol{u} + 2(B\rho)'\boldsymbol{u}' + B\rho\boldsymbol{u}'' = \left(\frac{1}{v}\right)'\boldsymbol{e} + \left(\frac{1}{v}\right)\boldsymbol{e}'\\
&\qquad\qquad + (\boldsymbol{u}\times\boldsymbol{b})',\\
&(B\rho)'''\boldsymbol{u} + 3(B\rho)''\boldsymbol{u}' + 3(B\rho)'\boldsymbol{u}'' + B\rho\boldsymbol{u}'''\\
&\quad = \left(\frac{1}{v}\right)''\boldsymbol{e} + 2\left(\frac{1}{v}\right)'\boldsymbol{e}' + \left(\frac{1}{v}\right)\boldsymbol{e}'' + (\boldsymbol{u}\times\boldsymbol{b})'',\\
&(B\rho)''''\boldsymbol{u} + 4(B\rho)'''\boldsymbol{u}' + 6(B\rho)''\boldsymbol{u}'' + 4(B\rho)'\boldsymbol{u}'''\\
&\quad + B\rho\boldsymbol{u}'''' = \left(\frac{1}{v}\right)'''\boldsymbol{e} + 3\left(\frac{1}{v}\right)''\boldsymbol{e}' + 3\left(\frac{1}{v}\right)'\boldsymbol{e}''\\
&\qquad\qquad + \frac{1}{v}\boldsymbol{e}''' + (\boldsymbol{u}\times\boldsymbol{b})''',
\end{aligned}
\tag{8}
$$

that provide the derivatives $\mathrm{d}^n\boldsymbol{u}/\mathrm{d}s^n$ needed in the Taylor expansions (4):

$$
\begin{aligned}
\boldsymbol{u}' &= \left(\frac{1}{v}\right)\boldsymbol{E} + (\boldsymbol{u}\times\boldsymbol{B}) - \frac{(B\rho)'}{B\rho}\boldsymbol{u}\\
\boldsymbol{u}'' &= \left(\frac{1}{v}\right)'\boldsymbol{E} + \left(\frac{1}{v}\right)\boldsymbol{E}'\Big|_{B\rho} + (\boldsymbol{u}\times\boldsymbol{B})'\big|_{B\rho} - 2\frac{(B\rho)'}{B\rho}\boldsymbol{u}'\\
&\quad - \frac{(B\rho)''}{B\rho}\boldsymbol{u},\\
\boldsymbol{u}''' &= \left(\frac{1}{v}\right)''\boldsymbol{E} + 2\left(\frac{1}{v}\right)'\boldsymbol{E}'\Big|_{B\rho} + \left(\frac{1}{v}\right)\boldsymbol{E}''\Big|_{B\rho} + (\boldsymbol{u}\times\boldsymbol{B})''|_{B\rho}\\
&\quad - 3\frac{(B\rho)'}{B\rho}\boldsymbol{u}'' - 3\frac{(B\rho)''}{B\rho}\boldsymbol{u}' - \frac{(B\rho)'''}{B\rho}\boldsymbol{u},\\
\boldsymbol{u}'''' &= \left(\frac{1}{v}\right)'''\boldsymbol{E} + 3\left(\frac{1}{v}\right)''\boldsymbol{E}'\Big|_{B\rho} + 3\left(\frac{1}{v}\right)'\boldsymbol{E}''\Big|_{B\rho}\\
&\quad + \left(\frac{1}{v}\right)\boldsymbol{E}'''\Big|_{B\rho} + (\boldsymbol{u}\times\boldsymbol{B})'''|_{B\rho} - 4\frac{(B\rho)'}{B\rho}\boldsymbol{u}'''\\
&\quad - 6\frac{(B\rho)''}{B\rho}\boldsymbol{u}'' - 4\frac{(B\rho)'''}{B\rho}\boldsymbol{u}' - \frac{(B\rho)''''}{B\rho}\boldsymbol{u},
\end{aligned}
\tag{9}
$$

where $\boldsymbol{E} = \boldsymbol{e}/B\rho$, $\boldsymbol{B} = \boldsymbol{b}/B\rho$, and $^{(n)}|_{B\rho}$ denotes differentiation at constant $B\rho$:

$$
\boldsymbol{E}^{(n)}|_{B\rho} = \frac{1}{B\rho}\frac{\mathrm{d}^n\boldsymbol{e}}{\mathrm{d}s^n} \quad \text{and}
$$

$$
(\boldsymbol{u}\times\boldsymbol{B})^{(n)}|_{B\rho} = \frac{1}{B\rho}(\boldsymbol{u}\times\boldsymbol{b})^{(n)}. \tag{10}
$$

The derivatives $\boldsymbol{e}^{(n)}$ and $\boldsymbol{b}^{(n)}$ of the electric and magnetic fields are calculated from the vector fields $\boldsymbol{e}(x, y, z)$, $\boldsymbol{b}(x, y, z)$ and their derivatives $\partial^{i+j+k}\boldsymbol{e}/\partial x^i\partial y^j\partial z^k$ and $\partial^{i+j+k}\boldsymbol{b}/\partial x^i\partial y^j\partial z^k$ provided by routines of the code that are dedicated to the simulation of the optical elements of concern.

These Eqs. (9), as well as the calculation of the rigidity, following Eq. (5), involve derivatives $(B\rho)^{(n)} = \mathrm{d}^n(B\rho)/\mathrm{d}s^n$, which are obtained in the following way [4]. Considering that

$$
\frac{\mathrm{d}p^2}{\mathrm{d}t} = \frac{\mathrm{d}\boldsymbol{p}^2}{\mathrm{d}t}, \quad \text{i.e.,} \quad \frac{\mathrm{d}p}{\mathrm{d}t}p = \frac{\mathrm{d}\boldsymbol{p}}{\mathrm{d}t}\boldsymbol{p}, \tag{11}
$$

we obtain (Eq. (2))

$$
\frac{\mathrm{d}p}{\mathrm{d}t}p = q(\boldsymbol{e} + v\times\boldsymbol{b})\cdot\boldsymbol{p} = q\boldsymbol{e}\cdot\boldsymbol{p}, \tag{12}
$$

since $(\boldsymbol{v}\times\boldsymbol{b})\cdot\boldsymbol{p} = 0$. Normalizing as previously with $\boldsymbol{p} = p\boldsymbol{u} = qB\rho\boldsymbol{u}$ and $\mathrm{d}s = v\,\mathrm{d}t$, and by successive differentiations, Eq. (12) leads to the $(B\rho)^{(n)}$

$$
\begin{aligned}
&(B\rho)' = \frac{1}{v}(\boldsymbol{e}\cdot\boldsymbol{u}),\\
&(B\rho)'' = \left(\frac{1}{v}\right)'(\boldsymbol{e}\cdot\boldsymbol{u}) + \frac{1}{v}(\boldsymbol{e}\cdot\boldsymbol{u})',\\
&(B\rho)''' = \left(\frac{1}{v}\right)''(\boldsymbol{e}\cdot\boldsymbol{u}) + 2\left(\frac{1}{v}\right)'(\boldsymbol{e}\cdot\boldsymbol{u})' + \frac{1}{v}(\boldsymbol{e}\cdot\boldsymbol{u})'',\\
&(B\rho)'''' = \left(\frac{1}{v}\right)'''(\boldsymbol{e}\cdot\boldsymbol{u}) + 3\left(\frac{1}{v}\right)''(\boldsymbol{e}\cdot\boldsymbol{u})'\\
&\qquad + 3\left(\frac{1}{v}\right)'(\boldsymbol{e}\cdot\boldsymbol{u})'' + \frac{1}{v}(\boldsymbol{e}\cdot\boldsymbol{u})'''.
\end{aligned}
\tag{13}
$$

Note that the $(\boldsymbol{e}\cdot\boldsymbol{u})^{(n)} = \mathrm{d}^n(\boldsymbol{e}\cdot\boldsymbol{u})/\mathrm{d}s^n$ can be related to the derivatives of the kinetic energy W by

$$\mathrm{d}W = \frac{\mathrm{d}\boldsymbol{p}}{\mathrm{d}t}\cdot\boldsymbol{v}\,\mathrm{d}t = q\boldsymbol{e}\cdot\boldsymbol{v}\,\mathrm{d}t,$$

which, by noting $\mathrm{d}s = v\mathrm{d}t$ and $\boldsymbol{u} = \boldsymbol{v}/v$, gives $\mathrm{d}^{n+1}W/\mathrm{d}s^{n+1} = q(\mathrm{d}^n(\boldsymbol{e}\cdot\boldsymbol{u})/\mathrm{d}s^n)$.

Finally, the derivatives $(1/v)^{(n)} = \mathrm{d}^n(1/v)/\mathrm{d}s^n$ involved in Eqs (9 and 13) are obtained from $p = (v/c)(W + mc^2/c$ (m = mass of the particle), by successive differentiations, that give (with $p = qB\rho$) the recursive relations

$$\left(\frac{1}{v}\right) = \frac{1}{c^2}\frac{W+mc^2}{qB\rho},$$

$$\left(\frac{1}{v}\right)' = \frac{1}{c^2}\frac{(\boldsymbol{e}\cdot\boldsymbol{u})}{B\rho} - \frac{1}{v}\frac{(B\rho)'}{B\rho},$$

$$\left(\frac{1}{v}\right)'' = \frac{1}{c^2}\frac{(\boldsymbol{e}\cdot\boldsymbol{u})'}{B\rho} - 2\left(\frac{1}{v}\right)'\frac{(B\rho)'}{B\rho} - \frac{1}{v}\frac{(B\rho)''}{B\rho},$$

$$\left(\frac{1}{v}\right)''' = \frac{1}{c^2}\frac{(\boldsymbol{e}\cdot\boldsymbol{u})''}{B\rho} - 3\left(\frac{1}{v}\right)''\frac{(B\rho)'}{B\rho} - 3\left(\frac{1}{v}\right)'\frac{(B\rho)''}{B\rho} - \frac{1}{v}\frac{(B\rho)'''}{B\rho}. \tag{14}$$

2.3. Integration in electric fields

The formalism is a simplified version of what has been exposed in the previous section, assuming that $\boldsymbol{b} = 0$. The equation of motion (3) then reduces to

$$(B\rho)'\boldsymbol{u} + B\rho\boldsymbol{u}' = \frac{\boldsymbol{e}}{v}, \tag{15}$$

and successive differentiations give the recursive relations

$$(B\rho)'\boldsymbol{u} + B\rho\boldsymbol{u}' = \frac{\boldsymbol{e}}{v},$$

$$(B\rho)''\boldsymbol{u} + 2(B\rho)'\boldsymbol{u}' + B\rho\boldsymbol{u}'' = \left(\frac{1}{v}\right)'\boldsymbol{e} + \frac{\boldsymbol{e}'}{v},$$

$$(B\rho)'''\boldsymbol{u} + 3(B\rho)''\boldsymbol{u}' + 3(B\rho)'\boldsymbol{u}'' + B\rho\boldsymbol{u}''' = \left(\frac{1}{v}\right)''\boldsymbol{e} + 2\left(\frac{1}{v}\right)'\boldsymbol{e}' + \left(\frac{1}{v}\right)\boldsymbol{e}'',$$

$$(B\rho)''''\boldsymbol{u} + 4(B\rho)'''\boldsymbol{u}' + 6(B\rho)''\boldsymbol{u}'' + 4(B\rho)'\boldsymbol{u}''' + B\rho\boldsymbol{u}'''' = \left(\frac{1}{v}\right)'''\boldsymbol{e} + 3\left(\frac{1}{v}\right)''\boldsymbol{e}' + 3\left(\frac{1}{v}\right)'\boldsymbol{e}'' + \left(\frac{1}{v}\right)'''\boldsymbol{e}''', \tag{16}$$

that provide the derivatives $\mathrm{d}^n\boldsymbol{u}/\mathrm{d}s^n$ needed in the Taylor expansions (4):

$$\boldsymbol{u}' = \left(\frac{1}{v}\right)\boldsymbol{E} - \frac{(B\rho)'}{B\rho}\boldsymbol{u},$$

$$\boldsymbol{u}'' = \left(\frac{1}{v}\right)'\boldsymbol{E} + \left(\frac{1}{v}\right)\boldsymbol{E}'\Big|_{B\rho} - 2\frac{(B\rho)'}{B\rho}\boldsymbol{u}' - \frac{(B\rho)''}{B\rho}\boldsymbol{u},$$

$$\boldsymbol{u}''' = \left(\frac{1}{v}\right)''\boldsymbol{E} + 2\left(\frac{1}{v}\right)'\boldsymbol{E}'\Big|_{B\rho} + \frac{1}{v}\boldsymbol{E}''\Big|_{B\rho} - 3\frac{(B\rho)'}{B\rho}\boldsymbol{u}'' - 3\frac{(B\rho)''}{B\rho}\boldsymbol{u}' - \frac{(B\rho)'''}{B\rho}\boldsymbol{u},$$

$$\boldsymbol{u}'''' = \left(\frac{1}{v}\right)'''\boldsymbol{E} + 3\left(\frac{1}{v}\right)''\boldsymbol{E}'\Big|_{B\rho} + 3\left(\frac{1}{v}\right)'\boldsymbol{E}''\Big|_{B\rho} + \left(\frac{1}{v}\right)\boldsymbol{E}'''\Big|_{B\rho} - 4\frac{(B\rho)'}{B\rho}\boldsymbol{u}''' - 6\frac{(B\rho)''}{B\rho}\boldsymbol{u}'' - 4\frac{(B\rho)'''}{B\rho}\boldsymbol{u}' - \frac{(B\rho)''''}{B\rho}\boldsymbol{u}, \tag{17}$$

where $\boldsymbol{E} = e/B\rho$, and $^{(n)}|B\rho$ denotes differentiation at constant $B\rho$: $\boldsymbol{E}^{(n)}|_{B\rho} = (1/B\rho)(\mathrm{d}^n\boldsymbol{e}/\mathrm{d}s^n)$. These derivatives of the electric field are provided by the program as mentioned in the previous section.

The derivatives of $B\rho$ and $(1/v)$ are obtained as described in Eqs. (11)–(14).

3. Optical elements: validation of the method

Two different means are available for introducing new optical elements in the code Zgoubi: either analytical models, or a treatment of field maps. Each one of these has been exploited for introducing first samples of electric and electro-magnetic devices, four of which are described in the next four sections; relevant numerical simulations, have been performed, in order to validate the method of integration thus implemented in Zgoubi.

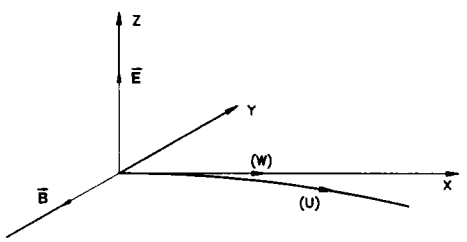

Fig. 2. Principle of the Wien filter (vertical separation). Trajectories of unwanted (U), and wanted (W) particles.

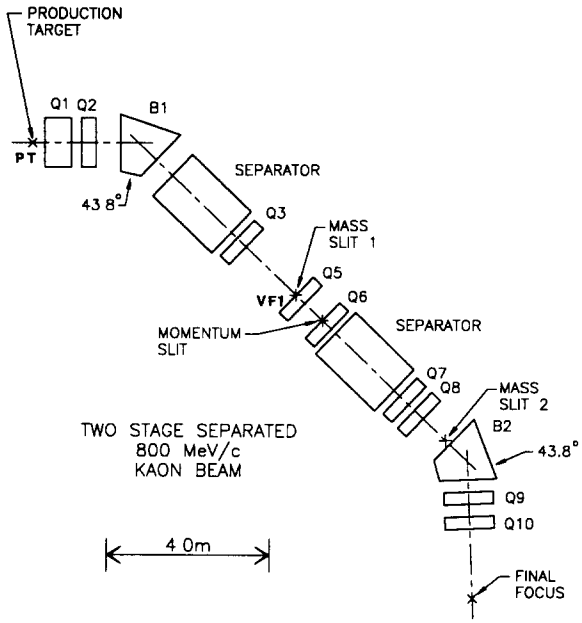

Fig. 3. Ray-tracing is performed in the first separation stage (from production target PT, to first vertical focus VF1) of an 800 MeV/c kaon beam line. The unwanted particles are 800 MeV/c pions. The motion in the 2.16 m long separator (Wien filter) is obtained from either an analytical solution of the cycloïdal motion, or numerical step by step integration (with ds steps of about 2 cm) in the crossed $\boldsymbol{e}$, $\boldsymbol{b}$ fields.

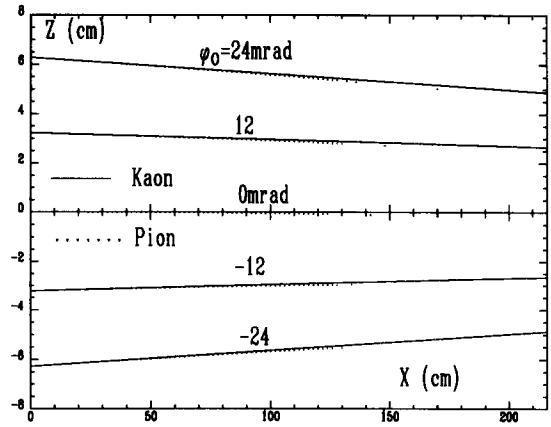

Fig. 4. Vertical projection (X–Z) of the trajectories of (unwanted) pions and (wanted) kaons in the Wien filter. Pions undergo a slight deflection that allows their separation at VF1, while kaons go straight. This process involves very small deflections, which dictates a high accuracy step by step integration procedure. The initial coordinates (at PT) are, $\theta_0 = 0$ and $\varphi_0 = 0, \pm 12, \pm 24$ mrad for kaons and pions.

3.1. Wien filter

The Wien filter (also known as velocity selector) is simulated by an analytical model of the field which consists of $\boldsymbol{e}$ and $\boldsymbol{b}$ components contained in the transverse plane, and orthogonal to each other (Fig. 2). Entrance and exit fringe fields can be simulated by means of a falloff of the form

$$F(d) = \frac{1}{1 + \exp(P(d))}, \tag{18}$$

where $P(d)$ is a polynomial to the fifth degree in d, distance from the effective field boundary (for more details, see ref. [2]).

In the constant field central region of the Wien filter, all derivatives of $\boldsymbol{e}$ and $\boldsymbol{b}$ (as involved in Eqs.

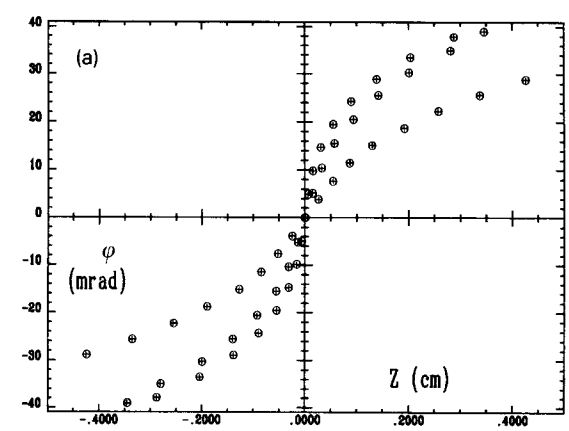

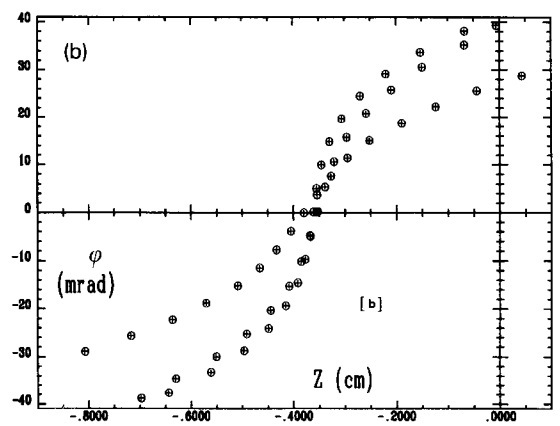

Fig. 5. Vertical phase-space coordinates after separation, at VF1, for (a) kaons ranging in $-24 \le \varphi_0 \le 24$ mrad, $\theta_0 = 0, \pm 200$ mrad, $y_0 = z_0 = 0$ initial coordinates (at PT, Fig. 3) and (b) pions in the same range. The z-separation appears to be $\simeq 0.37$ cm. The crosses (+) represent the result of the analytically solved cycloïdal motion, while the circles (○) result from the numerical step by step integration in the uniform $\boldsymbol{e}$, $\boldsymbol{b}$ field. Both methods are in perfect agreement, which validates the numerical one.

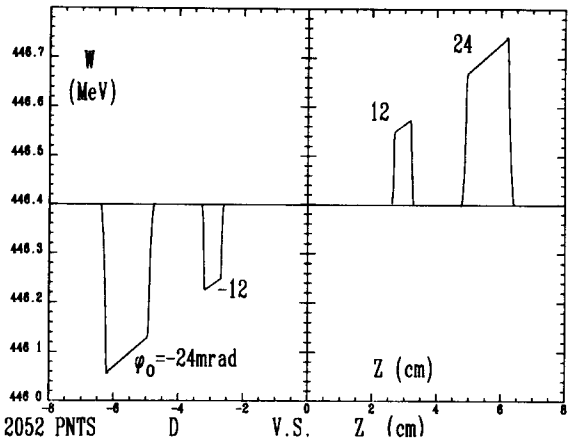

Fig. 6. A plot of the kinetic energy W inside the Wien filter vs z-elevation, of kaons issued from PT with initial coordinates $\theta_0 = 0$, $\varphi_0 = 0, \pm 12, \pm 24$ mrad (see their z-trajectories in Fig. 4). Entrance and exit fringe fields models following Eq. (19), are now taken into account. The variation of W along the Wien filter has been obtained from the fourth order Taylor expansion Eq. (5) and related Eqs. (11)–(14). In the uniform (inner) region, it appears to be linear, and in agreement with the relation $\Delta W = qe\Delta z$, with, here $qe = 5.5$ MeV/m. The extremely small variation of W (less than 1 keV per ds step) shows the high degree of precision obtained from the step by step integration in the crossed $\boldsymbol{e}$, $\boldsymbol{b}$ fields

(8)–(9) and (13)) are zero. In the entrance and exit field falloff regions the explicit derivatives of $\boldsymbol{e}$ and $\boldsymbol{b}$ with respect to the coordinates x, y, and z, are constitutive parts of the software definition of the element, and are derived from the expression of $F(d)$ (18).

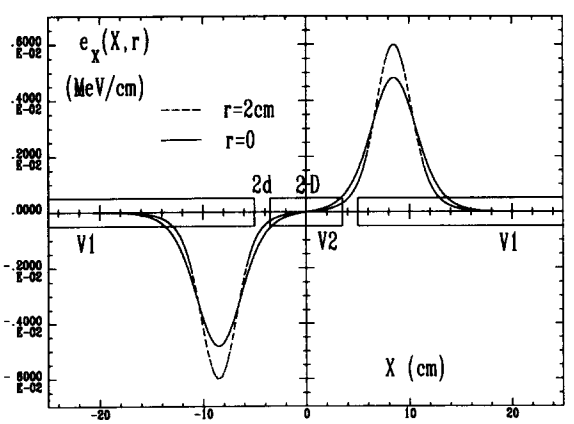

Fig. 7. Scheme of the unipotential electric lense, and longitudinal field component $e_x(x, r)$ along the lense axis ($r = 0$, solid line) and off-axis ($r = 2$ cm, dashed line) (Eqs. (19), (21)). In this example, we have taken $V_1 = 41.7$ kV; $V_2 = 13.44$ kV, $2d = 1.5$ cm, $2D = 7$ cm and $a = 3.5$ cm. The map mesh size is $\Delta X = 2$ mm for integration with Zgoubi.

For validating the step by step ray-tracing in such a device, a straightforward way consists in comparing the results thus obtained in a uniform field, by means of the optical element newly implemented in Zgoubi for this purpose, with the theoretical cycloïdal motion that constitutes the exact analytical solution of the differential equation of motion (2) in the case of the uniform field (such an analytical solution is already implemented in Zgoubi [2], which facilitates the comparison).

A synthesis of these results is given in Figs. 3–6 and their captions.

3.2. 1D axial field maps

Electric devices with cylindrical symmetry, such as unipotential lenses may be represented by the longitudinal component of $\boldsymbol{e}$ along the symmetry x-axis, namely $e(x, r = 0)$. Then, the longitudinal (x) and radial (r) field components off-axis are obtained by Taylor expansions (limited to the fifth degree in $r = (y^2 + z^2)^{1/2}$, which leads to high enough accuracy)

$$e_x(x, r) = e(x, 0) - \frac{r^2}{4}\frac{\partial^2 e}{\partial x^2}(x, 0) + \frac{r^4}{64}\frac{\partial^4 e}{\partial x^4}(x, 0),$$

$$e_r(x, r) = -\frac{r}{2}\frac{\partial e}{\partial x}(x, 0) + \frac{r^3}{16}\frac{\partial^3 e}{\partial x^3}(x, 0) - \frac{r^5}{384}\frac{\partial^5 e}{\partial x^5}(x, 0), \quad (19)$$

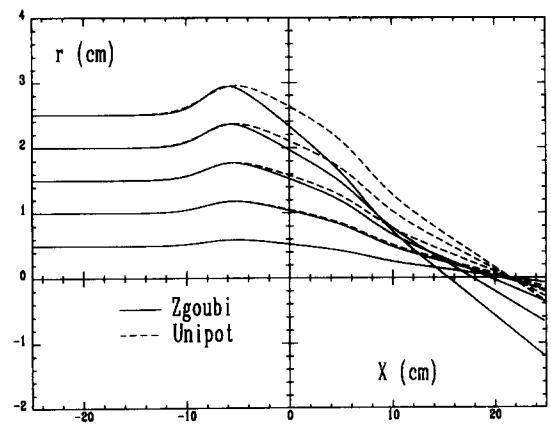

Fig. 8. Trajectories of protons of initial kinetic energy 41 7 kV ($B\rho = 0.02951$ Tm) in the unipotential lense. Solid lines: ray-tracing with Zgoubi. Dashed lines: integration of the linear first order differential Eq. (20) with UNIPOT. Nonlinearities appear to have an important effect as soon as $r_0 \gtrsim a/3.5 = 1$ cm, thus justifying numerical step by step integration of the exact equation of motion (2). The integration step size was $ds = 2$ mm with both codes, such a small value being dictated by the strong gradient between the electrodes.

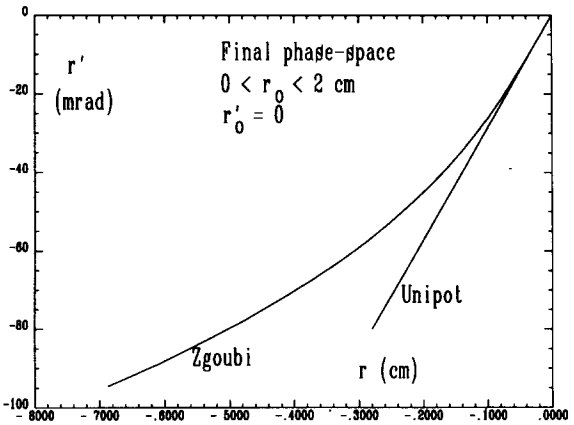

Fig. 9. Phase-space coordinates at the exit of the lense, following the results provided by Zgoubi and UNIPOT. As in the previous figure, the divergence between the linear approximation and the exact (numerical) solution appears to become important when $r_0 \gtrsim a/3.5 = 1$ cm.

which are next differentiated with respect to x, y or z in order to feed the Taylor series (17) that allow the numerical integration of the equation of motion (15).

The longitudinal field $e(x, 0)$ along the x-axis is in the present case provided to Zgoubi by means of a 1D field map (mesh size $\Delta x = 2$ mm). Then, the value of the field at any spot along the axis is given by an x-polynomial least-square fit interpolation. This polynomial is in turn differentiated in order to get the derivatives $\partial^n e/\partial x^n(x, 0)$ involved in the Taylor expansions above (19).

Ray-tracing calculations have been performed and compared with the results obtained from first order ray-tracing with a linear transport code, UNIPOT [5]

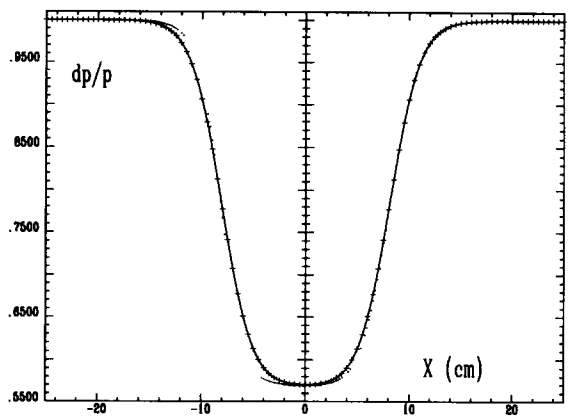

Fig. 10. Longitudinal component of the electric field as seen by a particle traversing the lense. Solid line: Zgoubi, $r_0 = 0$; dotted line: Zgoubi, $r_0 = 2$ cm; crosses: UNIPOT, whatever r_0.

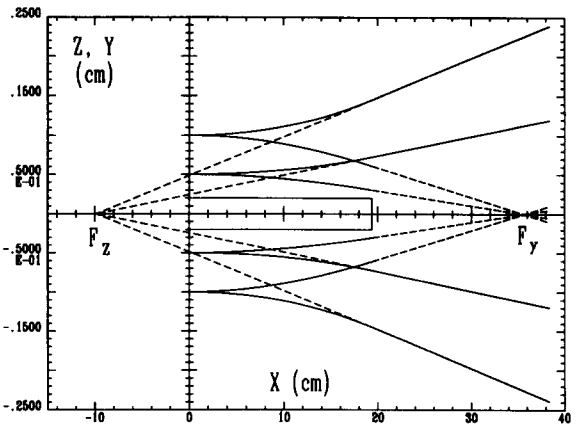

Fig. 11. Ray-tracing in the electric quadrupole. The quadrupole (symbolized by the rectangle) extends from $X = 0$ to $X = 19.4$ cm. Trajectories starting in the horizontal (respectively vertical) plane with $y_0 = \pm 0.5$ and ± 1 cm, and zero divergence (same in the z-plane) converge towards F_Y (respectively, are virtually issued from F_Z). The analytical formalism would give ref. [7], p. 341, distance from the exit face of quadrupole to $F_Y = \cos L\sqrt{K}/\sqrt{K}\sin L\sqrt{K} = 16.23$ cm (respectively, distance to $F_Z = \mathrm{ch}\, L\sqrt{K}/\sqrt{K}\,\mathrm{sh}\, L\sqrt{K} = 29.23$ cm) which is in perfect agreement with the results quoted here.

which solves the differential equation of motion

$$R'' + \frac{3}{16}\left[\frac{1}{V}\frac{\mathrm{d}V}{\mathrm{d}x}(x, 0)\right]^2 R = 0, \qquad (20)$$

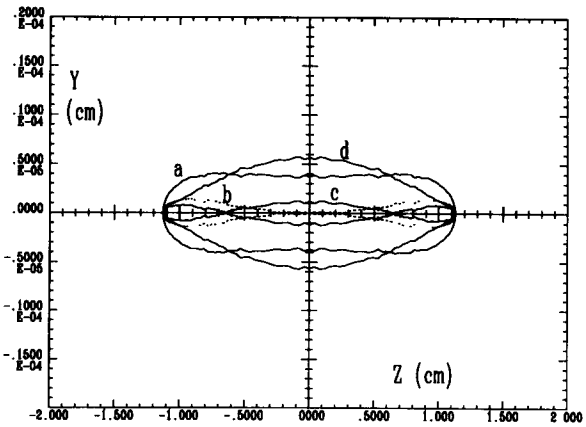

Fig. 12. Cross section of the image (showing the effect of the third order aberration) of a round hollow beam ($r_0 = \sqrt{y_0^2 + z_0^2} = 0.5$ cm), at the vicinity ΔX of the horizontal focus F_Y (Fig. 11) of the electric lense: (a) $\Delta X = -2$ μm; (b) $\Delta X = 0$; (c) $\Delta X = +0.06$ μm and (d) $\Delta X = +3$ μm. The same figures have been obtained in ref. [7], p. 343. Note the extreme accuracy of the ray-tracing, which is sensitive to such small ΔX shifts, while the ΔY distortion of the curves (attributed to the computer precision) appears to be much less than 10 nm.

Table 1
Transfer coefficients of Septier's electric quadrupole [7] as obtained from the analytical formalism ref. [8] p. 499, col. 1, and as provided by ray-tracing with Zgoubi, with either a sharp-edge field model (col. 2), or a model that includes a $2a \simeq 8\times10^{-2}$ m fringe field falloff (col. 3)

	Analytical formulae [8] [a] sharp edge field	From ray-tracing with Zgoubi	
		Sharp edge field model	With fringe field
(y/y)	0.6086	0.6086	0.6083
(y/θ)	0.1680	0.1680	0.1697
$(y/y\delta)$	0.7260	0.7273	0.7310
$(y/\theta\delta)$	0.0498	0.0499	0.0471
(θ/y)	−3.7487	−3.7487	−3.7136
(θ/θ)	0.6086	0.6086	0 6083
$(\theta/y\delta)$	6.3737	6.3750	6 2740
$(\theta/\theta\delta)$	0.7260	0.7274	0.7289
(z/z)	1.4502	1.4502	1.4495
(z/φ)	0.2223	0.2223	0.2200
$(z/z\delta)$	−0.9611	−0.9627	−0.9590
$(z/\varphi\delta)$	−0.0589	−0.0590	−0.0538
(φ/z)	4.9620	4.9619	5.0050
(φ/φ)	1.4502	1.4502	1.4495
$(\varphi/z\delta)$	−11.223	−11.220	−11.350
$(\varphi/\varphi\delta)$	−0.9611	−0.9627	−0.960
(x/yy)		0.5119	0.4985
$(x/y\theta)$	Not	−0.3148	−0.3206
$(x/\theta\theta)$	calculated	0.0740	0.0753
(x/zz)	in	0.6517	0.6181
$(x/z\varphi)$	ref. [8]	0.5221	0.510
$(x/\varphi\varphi)$		0.1247	0.1219

[a] Note that δ stands for $\delta W/W$ in ref. [8], while $\delta = \delta p/p$ in this report. The chromatic coefficients have therefore been converted by a factor of $\gamma + 1/\gamma \simeq 2$.

in the Picht variable $R = rV^{1/4}$ by means of a Runge–Kutta fourth order integration. For both codes Zgoubi and UNIPOT, the field $e(x, 0)$ on-axis was derived from a well-behaved model of scalar potential [5,6] (Fig. 7)

$$V(x,0) = \frac{V_2 - V_1}{4\omega d}\left[\ln\frac{\mathrm{ch}\frac{\omega(x+D+2d)}{a}}{\mathrm{ch}\frac{\omega(x+D)}{a}} + \ln\frac{\mathrm{ch}\frac{\omega(x-D-2d)}{a}}{\mathrm{ch}\frac{\omega(x-D)}{a}}\right], \quad (21)$$

such that $e(x, 0) = -(\mathrm{d}V/\mathrm{d}x)$. x is the distance from the center of the central electrode, V_1, V_2 are the potentials of the electrodes, $\omega = 1.318$, $2d$ = distance between the electrodes, $2D$ = length of the central electrode, a = inner radius of the electrodes.

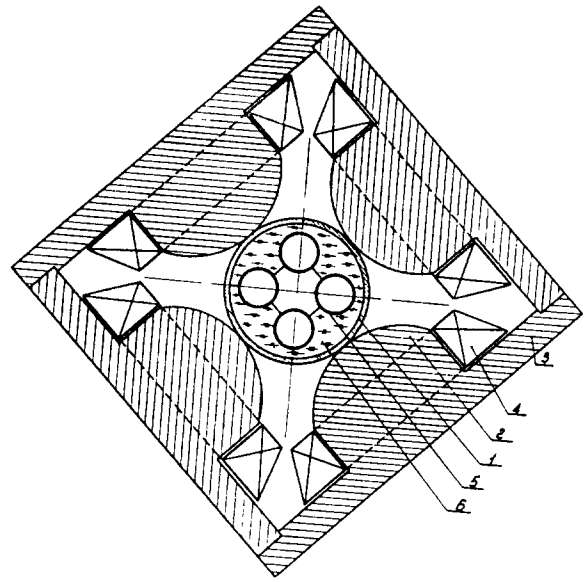

Fig 13. A scheme of the achromatic electromagnetic quadrupole (after ref. [9]): 1) vacuum pipe, 2) magnetic pole pieces, 3) return yoke, 4) coils, 5) electrodes, 6) plexiglas. In the text, the electrodes and the magnetic poles are assumed to present the same pole tip radius, $a = 4\times10^{-2}$ m, instead of what is schemed here. At the electrodes, $\phi = 714.2$ V, while at the magnetic poles $B = 0.03649$ T.

Table 2
Transfer coefficients of the achromatic quadrupole as obtained from the ray-tracing with Zgoubi, with either a sharp edge field model (col. 1) or a model that includes a $2a \simeq 8\times10^{-2}$ m fringe field falloff (the same for both electric and magnetic components) (col. 2). The comparison with the chromatic coefficients of the equivalent electric quadrupole (Table 1, cols. 2, 3) shows the expected effect of the combined fields on the transfer coefficients: the same first order focusing; and cancelling of the second order (chromatic) aberrations

	Sharp edge field model	With fringe field
(y/y)	0.6086	0.6077
(y/θ)	0.1680	0.1710
$(y/y\delta)$	-7×10^{-5}	7×10^{-4}
$(y/\theta\delta)$	-2×10^{-6}	-2×10^{-6}
(θ/y)	−3.7486	−3.6878
(θ/θ)	0.6086	0.6077
$(\theta/y\delta)$	-6×10^{-4}	6×10^{-3}
$(\theta/\theta\delta)$	-2×10^{-5}	-4×10^{-5}
(z/z)	1.4502	1.4486
(z/φ)	0.2223	0.2181
$(z/z\delta)$	10^{-4}	2×10^{-3}
$(z/\varphi\delta)$	3×10^{-6}	9×10^{-6}
(φ/z)	4.9618	5.0380
(φ/φ)	1 4502	1 4487
$(\varphi/z\delta)$	10^{-3}	2×10^{-2}
$(\varphi/\varphi\delta)$	4×10^{-5}	7×10^{-5}

A summary of the results, together with comments are given in Figs. 8–10 and their captions.

3.3. Electric quadrupole

In this example, we study the ray-tracing in an electric quadrupole. Substantial information is available from former publications we will refer to refs. [7,8], for the comparison with Zgoubi.

First, following ref. [7], we study some basic optical properties of a sharp edge field quadrupole characterized by an effective length $L = 19.4 \times 10^{-2}$ m and strength (in the nonrelativistic approximation) $K = \phi/a^2W = 22.319\ \mathrm{m}^{-2}$, in the particular case of protons (mass $m = 938.27\ \mathrm{MeV}/c^2$) of kinetic energy $W = 0.02$ MeV, giving the potential $\phi = 714.21$ V at a = pole tip radius $= 4 \times 10^{-2}$ m. The results are detailed in Figs. 11–12 and their captions. Second, we calculate (by ray-tracing sets of paraxial rays, see ref. [2]) the first and second order transfer coefficients of the lens (Ta-

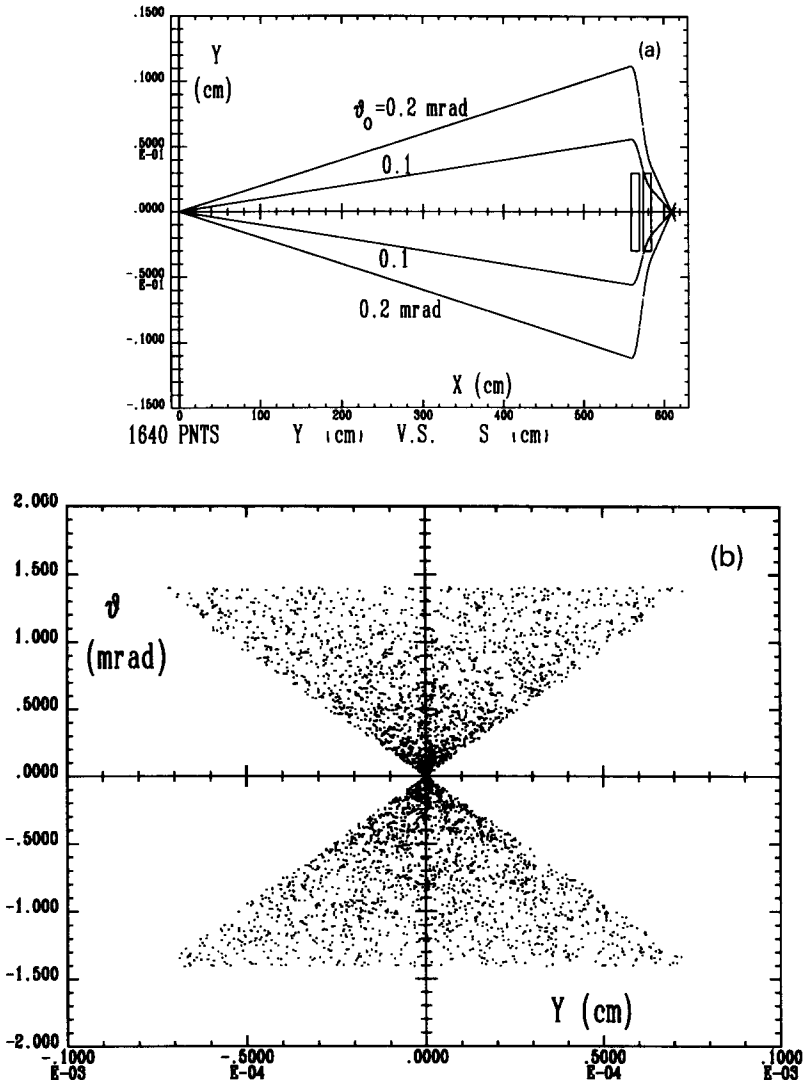

Fig. 14. Ray-tracing through a double focusing quadrupole doublet (typical of the front end design of microbeam lines). (a) a scheme of the trajectories, from the point object to the image plane; in the following, 4000 particles leave the point object within the acceptance $-0.2\ \mathrm{mrad} \le \theta_0 \le 0.2\ \mathrm{mrad}$ and $-0.2\ \mathrm{mrad} \le \varphi_0 \le 0.2\ \mathrm{mrad}$, with a (uniformly distributed) momentum dispersion $-3\times10^{-4} \le \delta p/p \le 3\times10^{-4}$. (b) the horizontal phase space (y, θ) shows the effect of the second order chromatic aberrations, linear in $\delta p/p$, and mostly responsible of (c) the image size, $\Delta Y_{\max}$ and $\Delta Z_{\max} \simeq \pm 0.7\ \mu$m, when using magnetic quadrupoles. (d) shows the drastic decrease of the image size when using an achromatic doublet – note the change in scales with respect to (c).

ble 1, col. 2) and show the excellent agreement with the analytical calculations of ref. [8] pp. 499 (Table 1, col. 1).

3.4. Achromatic quadrupole

The electromagnetic quadrupole combines electric and magnetic quadrupole fields [9] (Fig. 13). It has the special property that, in the case of nonrelativistic beams, it can be made achromatic to the second order so long as the electric and magnetic strengths

$$K_e = \frac{\phi}{a^2 W} \quad \text{and} \quad K_m = \frac{B}{aB\rho}$$

are related by

$$K_m = -2K_e.$$

Thus, referring to the previous example, an achromatic quadrupole having the same first order properties can

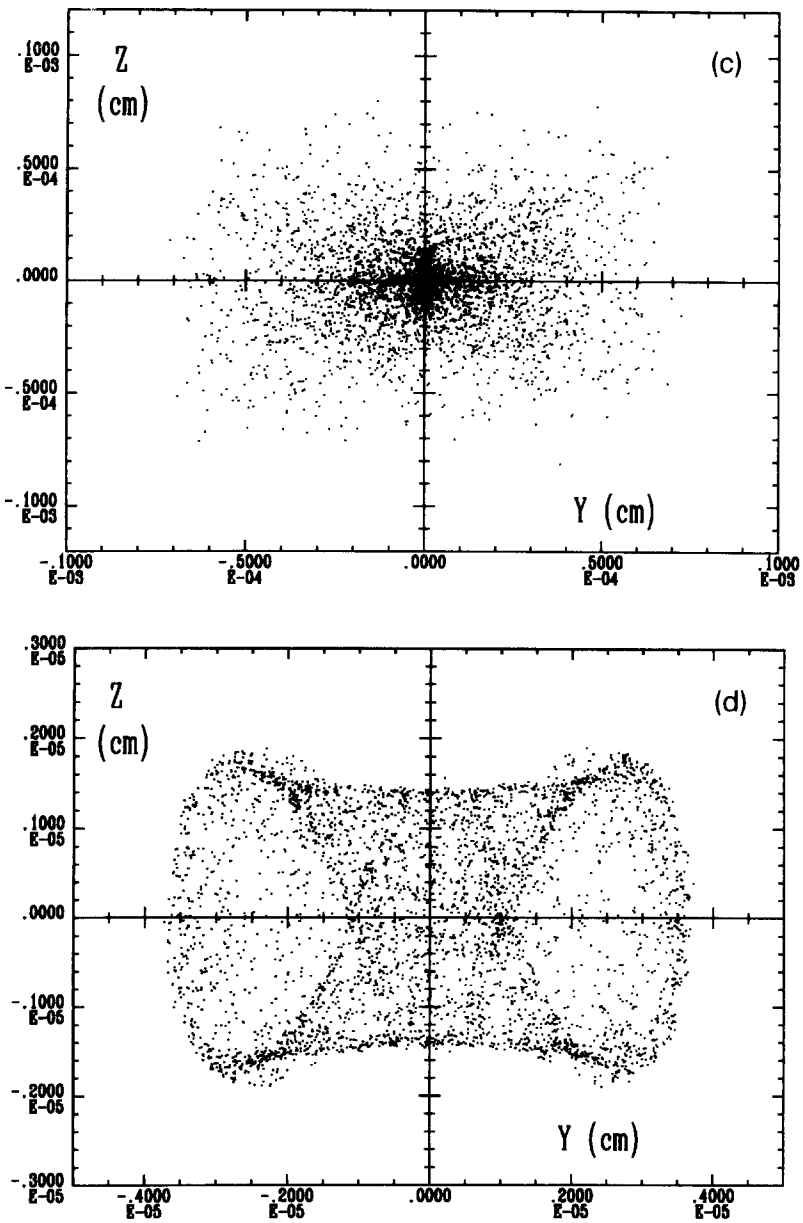

Fig. 14. Continued

```
MICROBEAM LINE, WITH AN ELECTROMAGNETIC QUADRUPOLE DOUBLET.
'MCOBJET'                                          RANDOM  OBJECT  DEFINITION.
20.435                                             RIGIDITY (20keV  PROTONS).
1                                                  UNIFORM IN WINDOW.
200                                                NUMBER  OF  PARTICLES.
0.      0.   0.   0.  1.                          CENTRAL  VALUE,  AND
0.      .2  .0    .2  0.0003                       HALF WIDTH OF DISTRIBUTION.
0.                                                 ZERO  LENGTH  OBJECT.
9   9. 9. 9. 9.                                    UNUSED.
186387 548728 472874                               SEEDS.
 'PARTICUL'                                        PARTICLE MASS AND CHARGE,
  938.2723 1.60217733E-19 0. 0. 0.                 FOR INTEGRATION IN E-FIELD.
'ESL'                                              DRIFT.
500.
'ESL'                                              DRIFT.
59.
'EBMULT'                                           FIRST ELECTROMAGNETIC
 0                                                                QUADRUPOLE.
10.2  10. 0. -9272.986  0. 0. 0. 0.                ELECTRIC Q-POLE COMPONENT.
 0.  0.  0.  0.  0.  0.  0.                        ENTRANCE EFB, SHARP EDGE.
6  .1122 6.2671 -1.4982 3.5882 -2.1209 1.723
 0.  0.  0.  0.  0.  0.  0.                        EXIT EFB, SHARP EDGE.
6  .1122 6.2671 -1.4982 3.5882 -2.1209 1.723
 0. 0. 0. 0. 0. 0.
10.2  10. 0.  1.89493  0. 0. 0. 0.                 MAGNETIC Q-POLE COMPONENT.
 0.  0.  0.  0.  0.  0.  0.                        ENTRANCE EFB, SHARP EDGE.
6  .1122 6.2671 -1.4982 3.5882 -2.1209 1.723
 0.  0.  0.  0.  0.  0.  0.                        EXIT EFB, SHARP EDGE.
6  .1122 6.2671 -1.4982 3.5882 -2.1209 1.723
0.  0. 0. 0. 0. 0.
.8
1 0. 0. 0.
'ESL'                                              DRIFT.
4.9
'EBMULT'                                           SECOND ELECTROMAGNETIC
 0                                                                QUADRUPOLE.
10.2  10. 0.  13779.90  0. 0. 0. 0.
 0.  0.  0.  0.  0.  0.  0.
6  .1122 6.2671 -1.4982 3.5882 -2.1209 1.723
 0.  0.  0.  0.  0.  0.  0.
6  .1122 6.2671 -1.4982 3.5882 -2.1209 1.723
0. 0. 0. 0. 0. 0.
10.2  10. 0.   -2.81592  0. 0. 0. 0.
 0.  0.  0.  0.  0.  0.  0.
6  .1122 6.2671 -1.4982 3.5882 -2.1209 1.723
 0.  0.  0.  0.  0.  0.  0.
6  .1122 6.2671 -1.4982 3.5882 -2.1209 1.723
0. 0. 0. 0. 0. 0.
.8
1 0. 0. 0.
'ESL'                                              DRIFT.
25.
'HISTO'                                            HISTOGRAM
2  -5E-6  5E-6     60  2                           OF THE Y COORDINATE.
20  'Y'  1  'Q'
'HISTO'                                            HISTOGRAM
4  -5E-6  5E-6     60  2                           OF THE Z COORDINATE.
20  'Z'  1  'Q'
'FAISCNL'                                          RAYS ARE STORED IN RAYS.OUT
RAYS.OUT                                           FOR FURTHER PLOTTING.
'REBELOTE'                                         RUN AGAIN, FOR RAYTRACING
19 0.1 0                                           200*(19+1) PARTICLES.
'FIN'
```

Fig. 15. The Zgoubi data file.

be realized by taking

$$K_e = \frac{\phi}{a^2 W} \quad \text{and} \quad K_m = -\frac{-2\phi}{a^2 W} \equiv \frac{-B}{aB\rho}.$$

Taking the same numerical values as in section 3.3, we obtain, for a sharp edge field model and with: $W = 0.02$ MeV (protons), $B\rho = 20.435 \times 10^{-3}$ T m, $K_m = -2K_e = 44.638$ m^{-2}, $\phi = -714.21$ V and $B = 0.036487$ T at pole tip radius $a = 4 \times 10^{-2}$ m.

Table 2 gives the resulting first and second order (chromatic) coefficients, here again obtained from the ray-tracing with Zgoubi, of an adequate set of paraxial rays. These chromatic coefficients now appear to be negligible, while the focusing properties of the lense are preserved with respect to the results of section 3.3, as was expected.

Finally, we illustrate these considerations by ray-tracing through a double focusing quadrupole doublet (Fig. 14a), and show the drastic decrease of the image size when using electromagnetic lenses instead of magnetic lenses (Figs. 14b–14d).

4. A specimen of input data formatting

The details of the contents and use of the ray-tracing code Zgoubi, as well as examples of input and output files, can be found in the up-to-date version of the Users' guide [10].

However, so as to illustrate this report and give an idea of the way a problem is treated with Zgoubi, a specimen of the input data file (whose logical name is normally ZGOUBI.DAT) for the ray-tracing of 4000 rays through the achromatic doublet (see section 3.4) is presented in Fig. 15 including comments for a better understanding of the description of the problem.

The results of the computations are normally printed in the output file of logical name ZGOUBI.RES, which we do not show here, because it is prohibitively long. Note that, as a consequence of the use of the special keyword "FAISCNL" in ZGOUBI.DAT, the 4000 rays are printed in the separate file RAYS.OUT rather than in ZGOUBI.RES. The Figs. 14a–14d were provided by further plotting of the content of RAYS.OUT by means of the dedicated Zgoubi graphic package. Various other forms of outputs are available (e.g. histograms of coordinates, spin components – when spin tracking is requested, first and higher order transfer coefficients), by means of dedicated keywords [10].

5. Conclusion

The ray-tracing and spin tracking code Zgoubi has been adapted and improved in order to allow ray-tracing in electric and combined electromagnetic fields, while its basic version was limited to the case of magnetic fields. These innovations have been tested by ray-tracing in newly implemented optical elements (Wien filter, unipotential lens, electric quadrupole, achromatic quadrupole). A detailed analysis of the results reveals the efficiency and high accuracy of the method of integration in all horizontal, vertical and longitudinal phase-spaces.

Acknowledgements

I wish to thank my colleagues G. Leleux and A. Tkatchenko for their help and the discussions.

References

[1] The basic version written for the purpose of spectrometer design at Saclay, is due to D. Garreta and J.C. Faivre, CEA-Saclay, early 1970's
[2] F. Méot and S. Valero, Zgoubi users' guide, Note SATURNE LNS/GT/90-05 (1990).
[3] F. Méot, A numerical method for the ray-tracing of polarized beams, Third European Particle Accelerator Conference, EPAC Berlin, 24–28 March 1992
[4] After discussions with G. Leleux, LNS, CEA-Saclay.
[5] Programme UNIPOT, A. Tkatchenko, SATURNE, CEA-Saclay, 1982.
[6] A. Septier, Cours de DEA de Physique des Particules, Année 1966–67, Université de Paris–Orsay; A.B. and J.C.J. El-Kareh, Electron beams, lenses, and optics, vol. 1 (Academic Press, New York and London, 1970).
[7] A. Septier and J. van Acker, Nucl. Instr. and Meth. 13 (1961) 335.
[8] Y. Fujita and H. Matsuda, Nucl. Instr. and Meth. 123 (1975) 495.
[9] S. Ya. Yavor et al., Nucl. Instr. and Meth. 26 (1964) 13.
[10] F. Méot and S. Valéro, Zgoubi users' guide, Version 3, Note SATURNE LNS/GT/93-12 (1993)